

Calcium-calmodulin does not alter the anion permeability of the mouse TMEM16A calcium-activated chloride channel

Yawei Yu, Ai-Seon Kuan, and Tsung-Yu Chen

Center for Neuroscience and Department of Neurology, University of California, Davis, Davis, CA 95618

The transmembrane protein TMEM16A forms a Ca^{2+} -activated Cl^- channel that is permeable to many anions, including SCN^- , I^- , Br^- , Cl^- , and HCO_3^- , and has been implicated in various physiological functions. Indeed, controlling anion permeation through the TMEM16A channel pore may be critical in regulating the pH of exocrine fluids such as the pancreatic juice. The anion permeability of the TMEM16A channel pore has recently been reported to be modulated by Ca^{2+} -calmodulin (CaCaM), such that the pore of the CaCaM-bound channel shows a reduced ability to discriminate between anions as measured by a shift of the reversal potential under bi-ionic conditions. Here, using a mouse TMEM16A clone that contains the two previously identified putative CaM-binding motifs, we were unable to demonstrate such CaCaM-dependent changes in the bi-ionic potential. We confirmed the activity of CaCaM used in our study by showing CaCaM modulation of the olfactory cyclic nucleotide-gated channel. We suspect that the different bi-ionic potentials that were obtained previously from whole-cell recordings in low and high intracellular $[\text{Ca}^{2+}]$ may result from different degrees of bi-ionic potential shift secondary to a series resistance problem, an ion accumulation effect, or both.

INTRODUCTION

The recently identified TMEM16 family encompasses transmembrane proteins of two functional categories: Ca^{2+} -activated ion channels (Hartzell, 2008; Huang et al., 2012a; Scudieri et al., 2012) and phospholipid scramblase (Suzuki et al., 2010, 2013; Yang et al., 2012; Malvezzi et al., 2013). Among these TMEM16 family members, TMEM16A and TMEM16B form Ca^{2+} -activated Cl^- channels (CaCCs) (Caputo et al., 2008; Schroeder et al., 2008; Yang et al., 2008), which are important for many physiological processes such as facilitating trans-epithelial Cl^- transport (Tarran et al., 2002; Huang et al., 2012b; Kunzelmann et al., 2012), controlling neuronal activity (Huang et al., 2012), and regulating smooth muscle contraction (Hwang et al., 2009; Bulley et al., 2012), to name a few. Although TMEM16A and TMEM16B both form CaCCs, these two anion channels appear to play separate physiological roles because of their different tissue distribution patterns. Generally speaking, TMEM16A is expressed abundantly in epithelial cells, whereas TMEM16B appears to express more in cells of neuronal origin. TMEM16B is known to be important for controlling the sensory signals of olfaction and vision (Stephan et al., 2009; Stöhr et al., 2009; Hengl et al., 2010), whereas TMEM16A is critical in controlling the transepithelial Cl^- transport (Tarran et al., 2002; Huang et al., 2012b; Kunzelmann et al., 2012).

The functional properties of CaCCs formed by TMEM16A and TMEM16B have been studied even

before their molecular cloning (Hartzell et al., 2005). These two Cl^- channels are activated by intracellular Ca^{2+} of submicromolar/micromolar concentrations (Qu and Hartzell, 2000, 2001). They allow various anions to permeate through the channel pore, including but not limited to SCN^- , I^- , NO_3^- , and Br^- . Various studies in the literature have shown that these anions all have higher permeability than Cl^- (namely, $P_X/P_{\text{Cl}} > 1$, where P_X represents the permeability of the anion X^-), with an established permeability sequence of $P_{\text{SCN}} > P_{\text{I}} \approx P_{\text{NO}_3} > P_{\text{Br}} > P_{\text{Cl}}$ (Qu and Hartzell, 2000; Ni et al., 2014). Besides these anions, TMEM16A is also permeable to HCO_3^- , a physiologically abundant anion (Qu and Hartzell, 2000; Jung et al., 2013; Ni et al., 2014). It has been suggested that TMEM16A and other anion transport proteins in pancreatic cells may be responsible for the high HCO_3^- concentration ($[\text{HCO}_3^-]$) (and therefore high pH) of the pancreatic juice (Sohma et al., 2001; Park and Lee, 2012).

Although the properties of CaCCs have been extensively studied, a controversy exists regarding the modulations of three biophysical properties of CaCC by calmodulin (CaM). First, it was reported that the activation of TMEM16A channel by intracellular Ca^{2+} requires CaM (Tian et al., 2011). Second, the binding of Ca^{2+} -CaM (CaCaM) to TMEM16A was shown to alter the permeability ratios of the channel to various anions

Correspondence to Tsung-Yu Chen: tyuchen@ucdavis.edu

Abbreviations used in this paper: CaCaM, Ca^{2+} -calmodulin; CaCC, Ca^{2+} -activated Cl^- channel; CaM, calmodulin.

© 2014 Yu et al. This article is distributed under the terms of an Attribution–Noncommercial–Share Alike–No Mirror Sites license for the first six months after the publication date (see <http://www.rupress.org/terms>). After six months it is available under a Creative Commons License (Attribution–Noncommercial–Share Alike 3.0 Unported license, as described at <http://creativecommons.org/licenses/by-nc-sa/3.0/>).

(Jung et al., 2013). Finally, the inactivation/desensitization (rundown) of the TMEM16 channel was thought to be mediated by CaCaM (Vocke et al., 2013). On the other hand, it has been shown that without CaCaM, the purified TMEM16A channel can still be activated by Ca^{2+} with an apparent affinity similar to those reported in the literature (Terashima et al., 2013). Another recent report also concluded that the activation of TMEM16A channel by Ca^{2+} is not mediated by CaM, and that adding CaCaM to the intracellular side of TMEM16A cannot recover or facilitate channel desensitization (rundown) (Yu et al., 2014). The biochemical assay in the latter two reports also showed that the binding of CaCaM to the TMEM16A channel protein was not significant (Terashima et al., 2013; Yu et al., 2014).

Thus, Terashima et al. (2013) and Yu et al. (2014) have provided functional data arguing against the requirement of CaCaM for channel activation or the involvement of CaCaM in channel rundown. However, these two studies did not address the effect of CaCaM on the anion permeability of TMEM16A reported by Jung et al. (2013). In this study, we examine specifically whether CaCaM can alter the anion permeability of the TMEM16A channel pore. We directly apply CaCaM to the cytoplasmic side of the TMEM16A channel and find that the bi-ionic potential of the TMEM16A current is not changed by CaCaM. Our results contradict those reported by Jung et al. (2013). We also noticed that the measured bi-ionic potential could significantly deviate from the true bi-ionic potential if the current amplitude was large, likely caused by series resistance and/or ion accumulation problems. These technical issues may undermine accurate patch-clamp measurements and consequently result in an artifactual alteration of the bi-ionic potentials reported by Jung et al. (2013).

MATERIALS AND METHODS

Molecular biology and channel expression

The mouse TMEM16A cDNA (RefSeq accession no. NM_001242349.1) was subcloned in the pEGFP-N3 vector or the IRES vector (Takara Bio Inc.). The former construct generated a TMEM16A channel protein with an enhanced green fluorescent protein (eGFP) attached to the C terminus. The IRES construct generated separate wild-type TMEM16A and eGFP molecules in the same transfected cells. Functional properties of the channels expressed from these two constructs were not differentiable. The principal subunit of the rat olfactory cyclic nucleotide-gated (CNCA2) channel (Dhallan et al., 1990) was subcloned in a modified pEGFP-N3 vector in which the eGFP was replaced with eYFP. Expression of TMEM16A channel and the homo-oligomeric CNCA2 channel was achieved by transfecting the respective cDNAs in human embryonic kidney 293 cells using lipofectamine transfection methods (Zhang et al., 2009; Richman et al., 2012; Ni et al., 2014). The transfected cells were identified by the green fluorescence in an inverted microscope (DM IRB; Leica) equipped with a fluorescent light source and a GFP filter (Chroma Technology Corp.). Electrophysiological recordings were performed within 24–72 h after transfections.

Electrophysiological experiments

Excised inside-out patch-clamp recordings were performed throughout the study. The extracellular (pipette) solution contained 140 mM NaCl, 10 mM HEPES, and 0.1 mM EGTA, pH 7.4. The intracellular (bath) solution contained 10 mM HEPES, 0.1 mM EGTA, and 140 mM sodium salt of Cl^- , I^- , or SCN^- , pH 7.4. Such solutions are defined as the “zero- Ca^{2+} ” solution because the added EGTA eliminates the contaminating Ca^{2+} in the solution. For intracellular solution containing HCO_3^- , 10 mM Cl^- was in the presence of 130 mM HCO_3^- . To activate TMEM16A channels, a total $[\text{Ca}^{2+}]$ of 120 μM was added to the zero- Ca^{2+} solution, leading to a free $[\text{Ca}^{2+}]$ of $\sim 20 \mu\text{M}$, a saturating $[\text{Ca}^{2+}]$. In several experiments, total $[\text{Ca}^{2+}]$ of 170 μM ($\sim 70 \mu\text{M}$ of free $[\text{Ca}^{2+}]$) was used, and no difference in the results was discerned. Borosilicate glass capillaries (World Precision Instruments) were used to fabricate the recording electrodes using an electrode puller (PP830; Narishige). The electrode resistance was ~ 1.5 – $2.5 \text{ M}\Omega$ when filled with the pipette solution. All experiments were performed using the Axopatch 200B amplifier controlled by Digidata1440 analogue–digital signal-converting board controlled by the pClamp10 software (Molecular Devices). Series resistance was not corrected.

The intracellular solution was delivered using a fast solution exchanger (SF-77; Warner Instruments) controlled by digital signals delivered by the Digidata 1440 board (Molecular Devices). The bi-ionic potential was measured under a condition in which 140 mM Cl^- was present in the extracellular side while 140 mM of another anion (X^-) was present in the intracellular side. An abbreviation of X^-/Cl^- represents such a bi-ionic condition. The ground electrode was placed in a reservoir containing 3 M KCl solution, which was connected to the bath (intracellular) solution via a 3-M KCl salt bridge. Junction potentials between NaCl and NaX solutions (140 mM) were small compared with the absolute values of the bi-ionic potential (Ni et al., 2014) and therefore were not corrected. The bi-ionic potential was measured in the presence of saturated intracellular $[\text{Ca}^{2+}]$, using either the voltage-clamp or the current-clamp ($I = 0$) methods described previously (Ni et al., 2014). In the current-clamp recording, the experiment started in 140 mM Cl^-/Cl^- condition, and the recorded voltage was normally close to 0 mV in this symmetrical Cl^- condition. When the intracellular Cl^- was replaced by a different anion X^- , the recorded voltage changed to the bi-ionic potential. The bi-ionic potential obtained from the current-clamp approach will be denoted as $E_{I=0}$. In voltage-clamp recordings, a voltage ramp from -80 to 80 mV or from 80 to -80 mV was applied for 3 s, and the reversal potential (denoted as E_{rev}) of the I-V curve was determined. Under the same bi-ionic condition, the value of $E_{I=0}$ in current-clamp ($I = 0$) experiments should in theory correspond to the value of E_{rev} in voltage-clamp experiments (Jung et al., 2013; Ni et al., 2014). The exchange of the intracellular solution was controlled by a 5-V digital signal from the Digidata 1440 board. Activation of the TMEM16A is demonstrated in Fig. 1 A. In short, an excised inside-out patch was positioned at the exit of the solution-delivery pipe delivering the zero- Ca^{2+} solution. The membrane potential was then clamped to $\pm 40 \text{ mV}$, followed by a switch of the intracellular solution to the one containing 20 μM $[\text{Ca}^{2+}]$. Normally, the solution exchange was completed in $< 100 \text{ ms}$ upon the change of the digital signal. Because the measured bi-ionic potential depended on the amplitude of the recorded current, we measured the current amplitude induced by 20 μM $[\text{Ca}^{2+}]$ at $\pm 40 \text{ mV}$ for every patch, either from experiments like that shown in Fig. 1 A or from the I-V curve obtained in symmetrical 140 mM $[\text{Cl}^-]$. The membrane conductance of the patch was thus estimated by dividing the current amplitude by the membrane voltage (40 mV).

To activate the olfactory CNCA2 channel, 2 μM cGMP (Sigma-Aldrich) was added to the 140-mM NaCl solution containing 20 μM of free $[\text{Ca}^{2+}]$. The membrane voltage of the excised inside-out

patch was held at 0 mV, and a 100-ms voltage pulse of 60 mV was delivered every 2 s. The switch of the intracellular solution from the zero-Ca²⁺ solution to the same solution containing 2 μM cGMP induced current through the open CNCA2 channel. CaM used in all experiments was the recombinant form purchased from Sigma-Aldrich. Stock CaM solutions of 60 μM were first made using the bath solutions (containing 120 μM of total [Ca²⁺]). CaM was then diluted 10-fold (6 μM) or 100-fold (0.6 μM) into the same bath solutions right before the experiments.

RESULTS

The TMEM16A Cl⁻ channel is opened by intracellular Ca²⁺, with a half-activation concentration of ~0.5 μM in the absence of Mg²⁺ (Ni et al., 2014). We examined the anion permeability of the mouse TMEM16A channel pore in the presence of saturating [Ca²⁺] (20 μM) throughout the study. Fig. 1 A illustrates the activation of Cl⁻ current, without added CaM, in an excised inside-out patch from human embryonic kidney 293 cells expressing TMEM16A. As the intracellular side of the membrane patch was exposed to Ca²⁺, the TMEM16A current was induced. The current disappeared quickly when intracellular Ca²⁺ was removed.

We measured bi-ionic potentials of the TMEM16A current with 20 μM of intracellular [Ca²⁺] using two different approaches: the current-clamp ($I = 0$) recording and the voltage-clamp recording (Ni et al., 2014). Fig. 1 B illustrates the current-clamp ($I = 0$) approach. In this experiment, the intracellular side of the patch was first exposed to the Cl⁻ solution with Ca²⁺. Because the extracellular and intracellular solutions contained nearly the same [Cl⁻], the recorded voltage ($E_{I=0}$) was close to 0 mV. As the intracellular solution was changed to a solution (with the same [Ca²⁺]) containing SCN⁻ or I⁻ of the same concentration as that of the extracellular Cl⁻, $E_{I=0}$ changed to a new value, which corresponds to the bi-ionic potential of SCN⁻/Cl⁻ or that of I⁻/Cl⁻. The measurement of bi-ionic potential by voltage-clamp recording is illustrated in Fig. 1 C. In this case, E_{rev} was determined from the I-V curve induced by a voltage ramp from -80 to 80 mV. For both the current-clamp and voltage-clamp experiments, the value of the measured bi-ionic potentials could vary from patch to patch, depending on the amplitude of the recorded current. For example, the current amplitudes of the two patches shown in Fig. 1 C differ by ~10-fold, and the measured

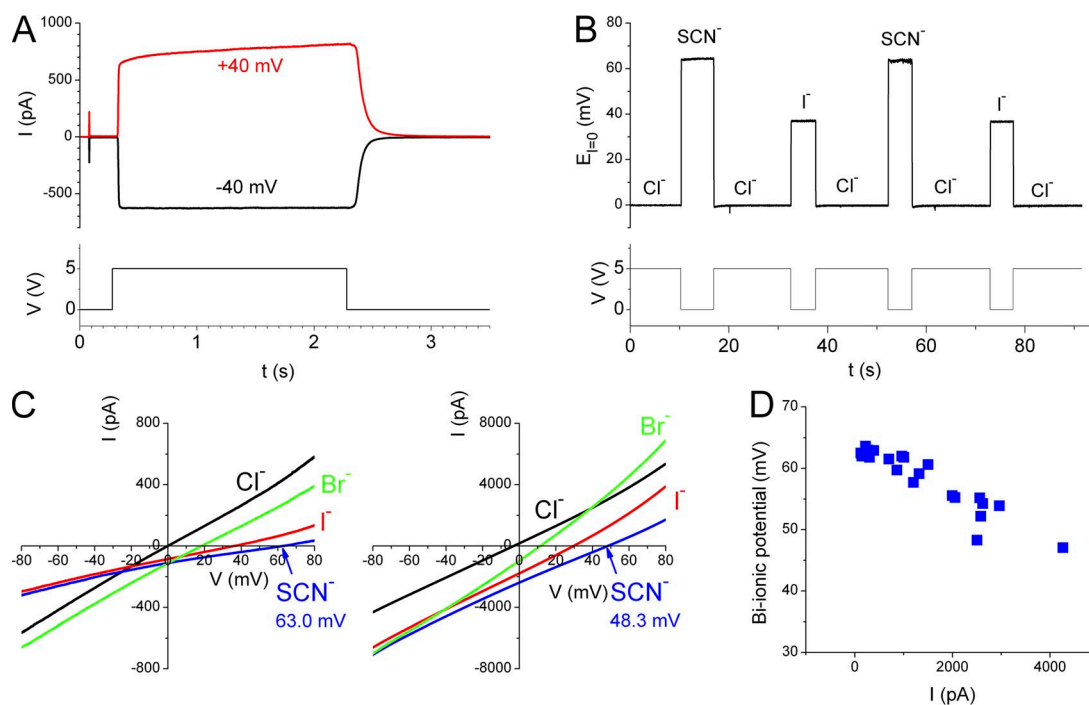


Figure 1. Measuring bi-ionic potential of the TMEM16A current. (A) Activation of Cl⁻ current (top) in an excised inside-out patch expressing TMEM16A in symmetrical 140 mM [Cl⁻]. (Bottom) The digital signal used to switch between the solutions containing zero-Ca²⁺ and 20 μM of free [Ca²⁺]. (B) Current-clamp ($I = 0$) recordings to monitor the change of bi-ionic potentials upon the switch of anion solutions on the intracellular side. Intracellular solutions contained 20 μM of free [Ca²⁺] throughout the recording. Same patch as in A. (Bottom) The digital signal for triggering solution exchange. (C) Bi-ionic potentials measured by voltage-clamp recordings. The two panels were recordings from two different patches consisting of currents of different amplitudes (see the scale of the y axis). Different values of E_{rev} were obtained as exemplified in the bi-ionic condition of SCN⁻/Cl⁻. (D) The SCN⁻/Cl⁻ bi-ionic potential as a function of the current amplitude at 40 mV in symmetrical 140 mM Cl⁻. Each data point was from an independent patch measured either by the voltage-clamp or by the current-clamp recording.

values of E_{rev} in the same SCN^-/Cl^- condition in these two patches are significantly different from each other. The bi-ionic potentials of SCN^-/Cl^- and I^-/Cl^- are ~ 60 – 65 mV and ~ 35 – 40 mV, respectively, when the recorded current at 40 mV in symmetrical 140 mM NaCl is <1 nA (Ni et al., 2014). As the current amplitude increases, the measured bi-ionic potential becomes smaller (Fig. 1 D).

Because the measured bi-ionic potential could vary with the amplitude of the recorded current, we avoided using the patches with current >1 – 1.5 nA at 40 mV for testing the CaCaM effect on the bi-ionic potential. Again, we used both the current-clamp and the voltage-clamp methods for testing the CaCaM effect. Fig. 2 A depicts the measurements of the bi-ionic potentials of SCN^-/Cl^- (top three panels) and I^-/Cl^- (bottom three panels) with and without CaCaM, using current-clamp (left) and voltage-clamp (two right panels) recordings. The current-clamp recordings, which monitored the bi-ionic potential in real time, did not reveal a change of $E_{I=0}$ after applying $0.6 \mu\text{M}$ CaCaM to the intracellular side of the patch for 2 min (Fig. 2 A, left). Similarly, the I-V curves in voltage-clamp recordings before and after

CaCaM application (two right panels in Fig. 2 A) did not show a significant difference in the measured values of E_{rev} . To fairly compare our results with those reported by Jung et al. (2013), we further increased the concentration of CaCaM to $6 \mu\text{M}$. Fig. 2 (B and C) shows that the values of $E_{I=0}$ are not affected by the presence of $6 \mu\text{M}$ of intracellular CaCaM in the bi-ionic condition of I^-/Cl^- (Fig. 2 B) or HCO_3^-/Cl^- (Fig. 2 C). Increasing free $[Ca^{2+}]$ to $70 \mu\text{M}$ in the presence of $6 \mu\text{M}$ CaM did not alter $E_{I=0}$ either (not depicted). These results contradicted the previous report by Jung et al. (2013) in which CaCaM was shown to alter the value of the bi-ionic potential when it was applied to the intracellular side of TMEM16A channels (see Fig. 4, D and E, of Jung et al., 2013). Because CaCaM failed to alter bi-ionic potentials in our experiments, we wondered if the mouse TMEM16A we used for the experiments contains the CaCaM-binding site identified by Jung et al. (2013). We therefore sequenced our TMEM16A clone, and the cDNA sequence indicated that the mouse TMEM16A clone used in this study does contain the two potential CaCaM-binding sites identified by Jung et al. (2013).

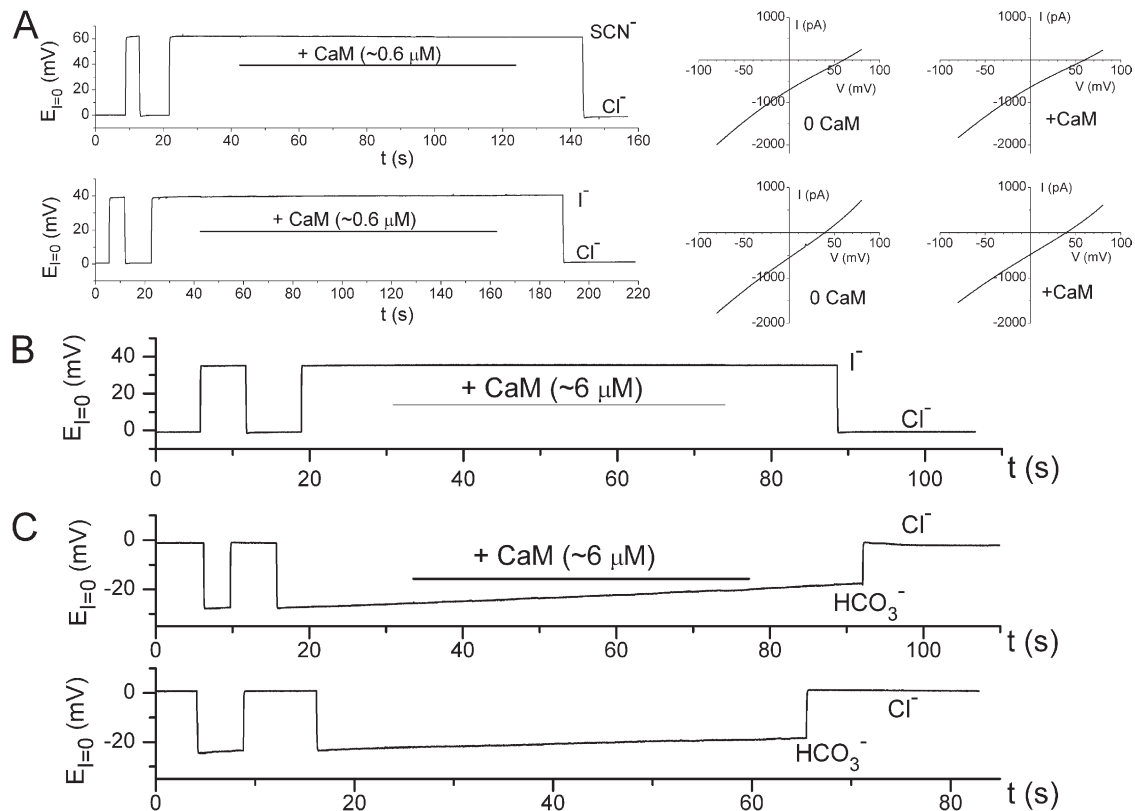


Figure 2. Applying CaCaM to the intracellular side of the TMEM16A channel does not alter the bi-ionic potential. All experiments were performed in inside-out patches. (A) Negative effect of CaCaM in altering the SCN^-/Cl^- and I^-/Cl^- bi-ionic potentials either from current-clamp (left) or from voltage-clamp (middle and right) measurements. Data in all panels were obtained from the same patch. 0.6 – $1.2 \mu\text{M}$ CaCaM was tested in more than 15 patches in various bi-ionic conditions without detectable effects on bi-ionic potentials. (B and C) CaCaM at a higher concentration did not alter the I^-/Cl^- bi-ionic potential (B) or the HCO_3^-/Cl^- bi-ionic potential (C, top). The slow change of the HCO_3^-/Cl^- bi-ionic potential also occurred without CaCaM (C, bottom). This is likely because of the combination of the changes of $[HCO_3^-]$ in the bath and the pipette solutions during prolonged recordings. $6 \mu\text{M}$ CaCaM was tested in three and eight separate experiments for I^-/Cl^- and HCO_3^-/Cl^- conditions, respectively, without detectable effects on $E_{I=0}$.

To demonstrate the effectiveness of CaCaM used in our study, we examined the effect of CaCaM on the cyclic nucleotide-gated channel, a well-documented effect (Chen and Yau, 1994; Chen et al., 1994). CaCaM was known to bind to the N-terminal cytoplasmic region of the CNCA2 channel (Liu et al., 1994), leading to a reduction of the apparent affinity of the channel for cGMP. Therefore, as the current of CNCA2 is activated by a nonsaturating concentration of cGMP, applying CaCaM to the cytoplasmic side of the channel should cause a current reduction. This was indeed observed in experiments illustrated in Fig. 3 in which the recorded CNCA2 current was potently inhibited by 0.6 μM CaCaM. As reported previously for CNCA2, when CaCaM was washed out in the presence of Ca^{2+} , the inhibited current was not recovered. It was only after the intracellular solution was changed to a zero- Ca^{2+} solution that the effect of CaCaM in inhibiting the olfactory cyclic nucleotide-gated channel was removed (Fig. 3). By reproducing the functional characteristics of the CaCaM modulation of the CNCA2 channel (Chen and Yau, 1994; Liu et al., 1994), we demonstrate that a lack of effect of CaCaM on TMEM16A is not caused by poor quality of CaM used in our studies.

Our experiments described above therefore do not support the conclusion that CaCaM alters the anion permeability of the TMEM16A. What then is the mechanistic basis underlying the finding of Jung et al. (2013) that the measured bi-ionic potentials are significantly

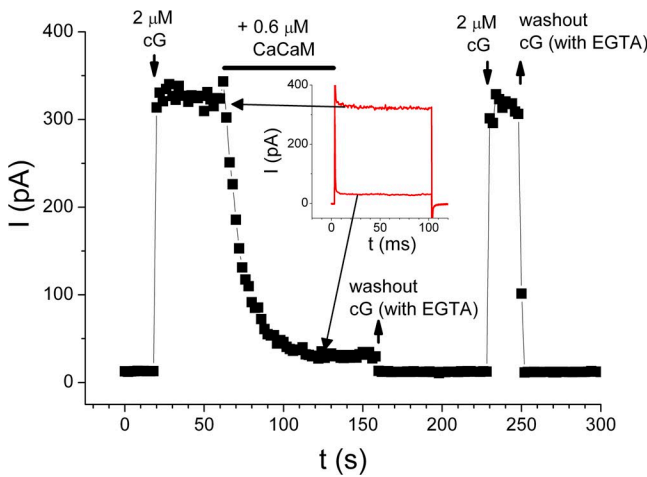


Figure 3. Effects of CaCaM on the homo-oligomeric CNCA2 olfactory cyclic nucleotide-gated channel. Black squares are the steady-state current measured at the end of the 100-ms voltage pulse. Inset shows the comparison of the recorded current traces before and during the application of CaM. The 2- μM cGMP solution contains 20 μM of free $[\text{Ca}^{2+}]$, whereas the 0-cGMP solution is the zero- Ca^{2+} solution containing 0.1 mM EGTA. After the current was inhibited by CaCaM, a washout of CaM in zero- Ca^{2+} solution at $t = 160$ s removed the binding of CaM, and the channel current was recovered as seen in the subsequent application of 2 μM cGMP. Positive CaCaM effects were found in all of seven independent experiments.

different between low and high $[\text{Ca}^{2+}]$ conditions in the whole-cell recording experiments (but not in the excised outside-out patch recordings)? We suspect that the precision of the bi-ionic potential measurement in Jung et al. (2013) might be limited by two factors: the series resistance problem and the ion accumulation effect, given the large current recorded in that study. Fig. 4 illustrates the series resistance problem, using the same set of data presented in Fig. 1 D. In an equivalent circuit shown in Fig. 4, the series resistance is related to the value of the true and measured bi-ionic potential according to the equation:

$$\begin{aligned}\varepsilon_m &= \varepsilon \cdot \left[\frac{R_m}{R_m + R_s} \right] \\ &= \varepsilon / \left[1 + (R_s/R_m) \right] \\ &= \varepsilon / \left[1 + (g_m/g_s) \right],\end{aligned}\quad (1)$$

where ε and ε_m are the true and measured bi-ionic potentials; R_m and R_s are the membrane resistance and the series resistance, respectively; and $g_m = 1/R_m$ and $g_s = 1/R_s$. We converted Fig. 1 D into a plot in which the measured bi-ionic potential is a function of g_m (Fig. 4). Fitting the data points in Fig. 4 to Eq. 1 gave the estimated values of $\varepsilon = 64.4$ mV and $g_s \approx 314$ nS (or $R_s = \sim 3.2$ M Ω). This analysis might overestimate the value of R_s because the change of bi-ionic potential was assumed to be all from the series resistance effect. Nonetheless, the

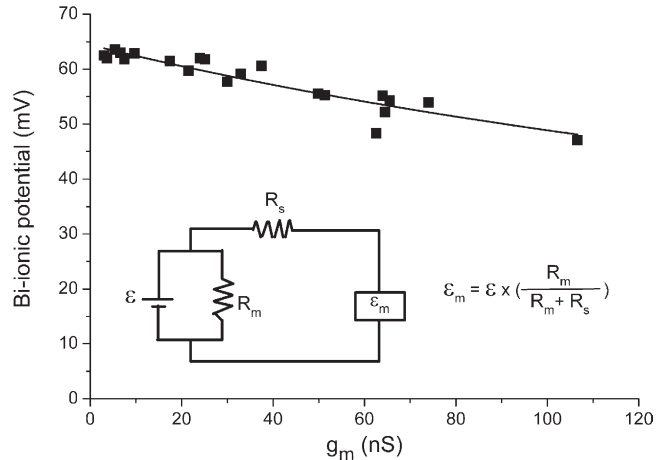


Figure 4. Measured bi-ionic potential (ε_m) as a function of membrane conductance. Data were the same as those shown in Fig. 1 D, except that the x-axis value of each data point was divided by 40 mV. Inset shows the equivalent circuit of the measurement of bi-ionic potential in which the true electromotive force (ε in inset) generated under a bi-ionic condition is detected as ε_m by the patch-clamp amplifier (represented by the square box) via a circuit containing a series resistance R_s . This series resistance demands that ε_m is a discounted value of ε according to Eq. 1. Fitting the data points to Eq. 1 allowed an estimation of the g_s , the inverse of which is the series resistance R_s . The data from this set of experiments were obtained from both voltage-ramp and current-clamp experiments, without paying attention to the ion accumulation effect as shown in Fig. 5.

estimated R_s value was reasonable given the resistance of the recording electrodes, suggesting that the series resistance indeed effectively reduced the bi-ionic potential as the membrane current increased.

Another factor that may significantly affect the measured bi-ionic potential is the accumulation of permeant ions as demonstrated in Fig. 5, in which the measured SCN^-/Cl^- bi-ionic potentials from the same patch using three methods are compared: the current-clamp ($I = 0$) method and two voltage-clamp recordings, one using a ramp voltage protocol from 80 to -80 mV and the other running in the reverse direction (from -80 to 80 mV). In voltage-clamp experiments, we switched the intracellular anion from Cl^- to SCN^- at 0 mV for several seconds before the start of the ramp protocol. As long as SCN^- was present in the intracellular side of the channel, an inevitable outward SCN^- flux would start an accumulation of SCN^- immediately adjacent to the membrane inside the pipette tip. A subsequent ramp protocol from -80 to 80 mV would exacerbate the SCN^- accumulation before the voltage reached the bi-ionic potential, whereas a voltage ramp in the reverse direction (80 to -80 mV) might partially alleviate the SCN^- accumulation. We compared the E_{rev} values from these two voltage-clamp measurements with the value of $E_{I=0}$ from the current-clamp experiment, in which the value of $E_{I=0}$ was determined immediately (<100 ms) after the intracellular solution was switched from Cl^- to SCN^- . Among these three methods, the current-clamp method gave the largest bi-ionic potential (Fig. 5 A, black squares), followed by the E_{rev} obtained with the ramp voltage from 80 to -80 mV (Fig. 5 A, blue squares), and then the E_{rev} from the ramp protocol of -80 to 80 mV (Fig. 5 A, red squares). Conceivably, the current-clamp method likely caused minimal ion accumulation because $E_{I=0}$ was determined immediately after the solution was switched. However, the bi-ionic potential still significantly decreased with an increase of g_m , even in this type of measurement (Fig. 5 A, black squares), likely caused by a series resistance problem. E_{rev} values of SCN^-/Cl^- obtained by the ramp protocol of 80 to -80 mV were nearly the same as the values of $E_{I=0}$ obtained from the current-clamp method in patches with small current. However, these two sets of data points (black and blue squares in Fig. 5 A) deviate from each other when the membrane current (or membrane conductance, g_m) is large. The values of E_{rev} obtained from the voltage ramp of -80 to 80 mV were always the smallest among the three measurements, and it appears that the higher the g_m (or membrane current), the larger the difference between the E_{rev} values obtained from ramp protocols running in opposite directions. These results suggest that the ion accumulation effect is more significant as the membrane current increases.

If ion accumulation is partially responsible for the difference of the measured bi-ionic potentials, the value of

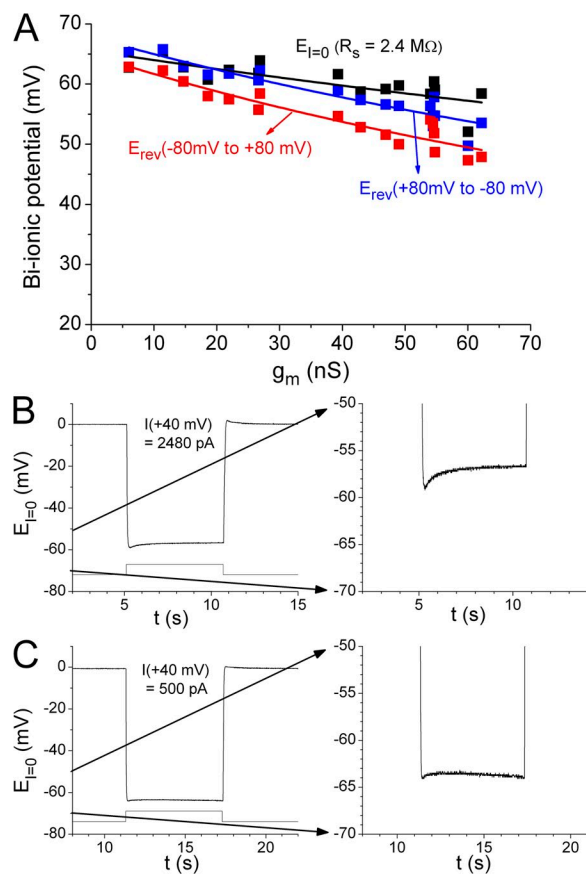


Figure 5. Ion accumulation changes the measured reversal potential under bi-ionic condition. (A) Comparison of the SCN^-/Cl^- bi-ionic potentials obtained from three different methods from the same patch. Data were from experiments different from those shown in Fig. 4. Data points with the same x-axis value were from the same patch. Data in black were obtained from the current-clamp ($I = 0$) method, measuring the peak value of $E_{I=0}$ immediately after the solution exchange from Cl^-/Cl^- to SCN^-/Cl^- . Data in blue and red were E_{rev} values measured from the voltage-ramp protocols from 80 to -80 mV and from -80 to 80 mV, respectively. The experiments from the same patch were always performed in a sequence so that the current-clamp experiment was performed first, followed by the voltage-ramp experiment from 80 to -80 mV, and then the ramp from -80 to 80 mV. Curve fitting to Eq. 1 for the bi-ionic potentials from the current-clamp experiments (black curve) gave an estimated R_s of 2.4 M Ω . Blue and red curves were also the best fit to Eq. 1, with fitted R_s values of 4.3 and 5.2 M Ω , respectively. These two fitted R_s values were likely overestimated because of the ion accumulation effect on top of the series resistance problem. (B) Time-dependent change of the measured $E_{I=0}$ upon switching the intracellular solution from Cl^- to SCN^- on a patch with large current. (Right) The expansion of the voltage range from -70 to -50 mV. From eight patches with $I_{+40\text{mV}}$ in the range of 1,150–2,480 pA, the difference between the peak $E_{I=0}$ and that measured at ~ 5 s after the SCN^- exposure was 2.2 ± 0.2 mV (mean \pm SEM). The fitted time constant of the relaxation was 635 ± 193 ms (mean \pm SEM). (C) Patches with small current showed larger absolute values of $E_{I=0}$ and less time-dependent changes of $E_{I=0}$. From patches with $I_{+40\text{mV}} = 250$ –600 pA, the difference between the $E_{I=0}$ values at the beginning and at 5 s after the SCN^- exposure was -0.1 ± 0.3 mV (mean \pm SEM; $n = 6$).

$E_{I=0}$ could change with time after switching solutions. Indeed, the absolute value of $E_{I=0}$ tends to decrease in patches with large current (Fig. 5 B), likely because of ion accumulation. For patches with smaller current (Fig. 5 C), the difference between the $E_{I=0}$ values at the beginning and at 5 s after SCN^- exposure was negligible, consistent with the results in Fig. 5 A showing that ion accumulation in patches with larger current could be more severe, and could be responsible for the bigger differences between bi-ionic potentials measured from different recording methods.

DISCUSSION

Anion permeation through various Cl^- channels is important for transepithelial transport and thus is critical for transepithelial fluid secretion. For example, a genetic defect of the Cl^- channel encoded by the CFTR gene is known to cause defective transepithelial fluid transport in the respiratory tract, leading to severe pulmonary infection in patients with cystic fibrosis (Boucher, 2007; Quinton, 2007). Because CaCC expresses in the same epithelial cells, it has been proposed that activation of CaCC may supplement the function of defective CFTR Cl^- channels, implicating a critical role of CaCC in transepithelial transport (Tarran et al., 2002; Cuthbert, 2011). Both CFTR and CaCC channel pores are permeable to HCO_3^- as well as to Cl^- . It is well established that a defective CFTR Cl^- channel can cause an abnormal pH of the pancreatic juice, which in normal human beings can contain up to 140 mM HCO_3^- (Kopelman et al., 1988; Scheele et al., 1996). Although the mechanism of producing such a high $[\text{HCO}_3^-]$ in pancreatic juice is not known, it is believed that such a HCO_3^- secretion mechanism may involve collective functions of CFTR, SLC26 $\text{Cl}^-/\text{HCO}_3^-$ antiporters, and TMEM16A-encoded CaCC (Sohma et al., 2001; Park and Lee, 2012).

Thus, a modulation of the anion permeability of the TMEM16A channel by CaCaM, as reported by Jung et al. (2013), could be physiologically important. Jung et al. (2013) showed a recording trace from an excised inside-out patch in which the $\text{HCO}_3^-/\text{Cl}^-$ bi-ionic potential was reduced to near 0 mV upon applying CaCaM to the intracellular side of the channel (Fig. 4 D of Jung et al., 2013). In contrast, we are unable to reproduce this CaCaM effect in similar experiments (Fig. 2). One might consider that the mouse TMEM16A clone used in our study and the human TMEM16A clone used in Jung et al. (2013) are different. However, the two cDNA clones express channels with very similar functional properties. Furthermore, the sequences of the two potential CaM-binding motifs identified by Jung et al. (2013) are nearly identical between the human and the mouse clones. For example, out of the 32 amino acids in CaM-binding motif 1, there are only two conserved amino acid changes (valine versus isoleucine or alanine). The

conserved valine/isoleucine variation also constitutes the only two amino acid differences in CaM-binding motif 2 between the two clones. It should be noted that various studies in the literature have presented either positive or negative biochemical evidence for CaCaM binding to TMEM16A, but there is no report that CaCaM binding to TMEM16 channels is species specific. Jung et al. (2013) and Vocke et al. (2013) showed that CaCaM binds to specific motifs in the human and rat clones, respectively, although the proposed CaCaM-binding site(s) in these two studies is not exactly the same. On the other hand, Terashima et al. (2013) reported that CaCaM interacts with human TMEM16A weakly, if at all. These authors also pointed out that TMEM16A is extremely sensitive to the detergent used for extraction from cell membranes. It is therefore possible that the detergent used to extract the protein might adversely affect the stability of the channel, leading to the exposure of domains that are inaccessible to CaM in a correctly folded TMEM16A protein (Terashima et al., 2013). Most recently, Yu et al. (2014) further compared side-by-side the experiments using human and mouse TMEM16A channels, and found no difference between CaCaM binding to mouse or to human clones; CaCaM binding to both clones was insignificant. Given these biochemical data in the literature, we do not think that the difference between our results and the electrophysiological results in Jung et al. (2013) can be attributed to the sequence difference in the potential CaCaM-binding motifs.

On the other hand, our study did demonstrate a problem of patch-clamp measurements well known in the literature: the accuracy of the voltage measurement depends on the size of the measured current (Sigworth, 1983; Sakmann and Neher, 1984). The I^-/Cl^- bi-ionic potentials measured in our laboratory were routinely in the range of 35 to 40 mV when the recorded current was <1 nA, corresponding to a $P_{\text{I}^-}/P_{\text{Cl}^-}$ permeability ratio of >4 (Ni et al., 2014). In the whole-cell recordings by Jung et al. (2013), the averaged permeability ratio of $P_{\text{I}^-}/P_{\text{Cl}^-}$ at low $[\text{Ca}^{2+}]$ (400 nM), which was thought to activate CaM only minimally, was <3 , whereas the averaged $P_{\text{I}^-}/P_{\text{Cl}^-}$ ratio was >4 from the excised outside-out patch recordings (Jung et al., 2013). Although the smaller value of $P_{\text{I}^-}/P_{\text{Cl}^-}$ in whole-cell recordings with 400 nM $[\text{Ca}^{2+}]$ might still be explained by a partial effect of CaCaM on the $P_{\text{I}^-}/P_{\text{Cl}^-}$ ratio, other factors, such as a large recorded current, could significantly affect the measured bi-ionic potentials. These other possibilities therefore deserve serious consideration. In patch-clamp recordings, the electrodes have finite resistance. The electrode resistance together with some less defined resistance generated during giga-seal formation contributes to most of the series resistance, which renders the command voltage sensed by the membrane patch, or conversely, the bi-ionic potential detected by the patch-clamp amplifier,

underestimated by a factor of $R_m/(R_m + R_s)$ (Fig. 4). If R_m is small relative to R_s , the measured bi-ionic potential will significantly deviate from the true value. As an example, the averaged resistance of our recording electrodes is $\sim 2\text{ M}\Omega$. A membrane current of 1 nA at 40 mV corresponds to an R_m value of 40 M Ω . The E_{rev} measured from such a membrane patch has already been underestimated by $\sim 5\%$! With a larger recorded current and/or a higher electrode resistance, the accuracy of the measurement would be worse. In Jung et al. (2013), one major experimental result arguing for the CaCaM effect was a difference of bi-ionic potentials between low and high intracellular $[\text{Ca}^{2+}]$ in whole-cell recording experiments. The amplitude of the recorded whole-cell currents shown in their study was routinely several nanoamperes or more, and the electrodes used had a resistance of 2–5 M Ω . Because the half-activating $[\text{Ca}^{2+}]$ for TMEM16A is $\sim 1\text{ }\mu\text{M}$ in the presence of 4 mM of intracellular $[\text{Mg}^{2+}]$ (Ni et al., 2014), a low (400 nM) and a high (3 μM) intracellular $[\text{Ca}^{2+}]$ in solutions with 4 mM $[\text{Mg}^{2+}]$ in Jung et al. (2013) must activate very different amplitudes of TMEM16A current. In these two $[\text{Ca}^{2+}]$ conditions, therefore, the series resistance likely alters the accuracy of voltage measurements to different degrees.

Besides the series resistance problem, ion accumulation can also potentially alter the measured bi-ionic potential. Even in our excised patch recording where the current is small compared with that of the whole-cell recording, reversing the direction of the voltage ramp results in an appreciable change of the measured E_{rev} . In Fig. 5 A, the SCN^-/Cl^- bi-ionic potential measured with the ramp protocol from -80 to 80 mV was consistently smaller than that obtained from the ramp running in the opposite direction. We reason that the voltage ramp from -80 to 80 mV, which first generates a negative current carried by an outward SCN^- flux, likely exacerbates local SCN^- accumulation in the pipette, whereas a reverse ramp direction could partially alleviate SCN^- accumulation. Furthermore, it appears that the higher the recorded membrane current, the larger the difference between the E_{rev} values obtained from voltage ramps running in different directions (Fig. 5 A). This ion accumulation can also be directly observed from the time-dependent change of the $E_{\text{I=0}}$ value in the current-clamp recordings (Fig. 5 B). In our excised patch recordings, the ion accumulation effect reached a steady state quickly (Fig. 5 B) and appeared to be smaller than the effect caused by the series resistance problem. Nonetheless, the ion accumulation problem could be significant in whole-cell voltage-clamp recordings. Vocke et al. (2013) has estimated that a Cl^- efflux from a spherical cell with a diameter of 10 μm caused by a decaying current of 1 nA can reduce the “effective” intracellular $[\text{Cl}^-]$ by 120 mM in 10 s! Because of the ion accumulation and the series resistance problem mentioned above, our study raises a serious concern regarding

the accuracy of bi-ionic potential measurements when the bi-ionic potentials to be compared are obtained from currents with vastly different amplitudes.

If the change of relative permeability calculated from bi-ionic potentials in Jung et al. (2013) was caused by technical issues of series resistance and/or ion accumulation as explained above, it might be puzzling why mutations in the putative CaM-binding domains could eliminate (or partially eliminate) the Ca^{2+} effect on the relative permeability, as shown in Figs. 5 and S8 of Jung et al. (2013). Based on our interpretation that the estimated relative permeability depends on the recorded current amplitude, we suspect that the CaM-binding domain mutations might reduce channel expression. Indeed, the representative recording traces in Fig. S8 of Jung et al. (2013) clearly show that the mutants have less current than the wild-type channel. Consistent with this interpretation, the half-effective $[\text{Ca}^{2+}]$ (EC50) in titrating the relative permeability of TMEM16A was estimated to be 0.91 μM (see Fig. 1 C of Jung et al., 2013). This value of EC50, which was interpreted as the Ca^{2+} affinity of CaM, was close to the EC50 of opening TMEM16A in the presence of $[\text{Mg}^{2+}]$ in the millimolar range (Xiao et al., 2011; Adomaviciene et al., 2013; Ni et al., 2014). We feel that the similarity in EC50s in controlling relative permeability as well as channel opening is not a coincidence. It is likely that the $[\text{Ca}^{2+}]$ -dependent change of relative permeability was in fact an epiphenomenon of the $[\text{Ca}^{2+}]$ -dependent activation of the TMEM16A channel but not an effect mediated by CaM.

Our study does not provide biochemical evidence as to whether or not CaCaM can directly bind to the TMEM16A channel protein. However, our electrophysiological recordings show that applying CaCaM directly to the cytoplasmic side of the TMEM16A channel in excised inside-out patch recordings does not alter the bi-ionic potential of the recorded current. We argue that the functional effect found in Jung et al. (2013)—namely, the difference of anion permeability ratios measured in different intracellular $[\text{Ca}^{2+}]$ in whole-cell recordings—may be explained by the series resistance problem and/or the ion accumulation effect. It will require more studies from different laboratories to resolve the controversy regarding the various CaCaM modulation effects on the TMEM16A channel.

We thank Dr. Wei-Ping Yu for subcloning the TMEM16A and the CNCA2 cDNAs. Special thanks go to Dr. Jeffrey Tang from Axon Instruments/Molecular Devices for a stimulating discussion on the series resistance problem. We also thank Drs. Robert Fairclough and Tzyh-Chang Hwang for critical reading of the manuscript.

This work was partially supported by National Institutes of Health grant R01GM065447.

The authors declare no competing financial interests.

Angus C. Nairn served as editor.

Submitted: 12 February 2014

Accepted: 9 June 2014

REFERENCES

- Adomaviciene, A., K.J. Smith, H. Garnett, and P. Tammaro. 2013. Putative pore-loops of TMEM16/anoctamin channels affect channel density in cell membranes. *J. Physiol.* 591:3487–3505. <http://dx.doi.org/10.1113/jphysiol.2013.251660>
- Boucher, R.C. 2007. Airway surface dehydration in cystic fibrosis: Pathogenesis and therapy. *Annu. Rev. Med.* 58:157–170. <http://dx.doi.org/10.1146/annurev.med.58.071905.105316>
- Bulley, S., Z.P. Neeb, S.K. Burris, J.P. Bannister, C.M. Thomas-Gatewood, W. Jangsangthong, and J.H. Jaggar. 2012. TMEM16A/ANO1 channels contribute to the myogenic response in cerebral arteries. *Circ. Res.* 111:1027–1036. <http://dx.doi.org/10.1161/CIRCRESAHA.112.277145>
- Caputo, A., E. Caci, L. Ferrera, N. Pedemonte, C. Barsanti, E. Sondo, U. Pfeiffer, R. Ravazzolo, O. Zegarra-Moran, and L.J. Galiotta. 2008. TMEM16A, a membrane protein associated with calcium-dependent chloride channel activity. *Science*. 322:590–594. <http://dx.doi.org/10.1126/science.1163518>
- Chen, T.Y., and K.W. Yau. 1994. Direct modulation by Ca^{2+} -calmodulin of cyclic nucleotide-activated channel of rat olfactory receptor neurons. *Nature*. 368:545–548. <http://dx.doi.org/10.1038/368545a0>
- Chen, T.Y., M. Illing, L.L. Molday, Y.T. Hsu, K.W. Yau, and R.S. Molday. 1994. Subunit 2 (or beta) of retinal rod cGMP-gated cation channel is a component of the 240-kDa channel-associated protein and mediates Ca^{2+} -calmodulin modulation. *Proc. Natl. Acad. Sci. USA*. 91:11757–11761. <http://dx.doi.org/10.1073/pnas.91.24.11757>
- Cuthbert, A.W. 2011. New horizons in the treatment of cystic fibrosis. *Br. J. Pharmacol.* 163:173–183. <http://dx.doi.org/10.1111/j.1476-5381.2010.01137.x>
- Dhallan, R.S., K.W. Yau, K.A. Schrader, and R.R. Reed. 1990. Primary structure and functional expression of a cyclic nucleotide-activated channel from olfactory neurons. *Nature*. 347:184–187. <http://dx.doi.org/10.1038/347184a0>
- Hartzell, H.C. 2008. Physiology. CaCl -ing channels get the last laugh. *Science*. 322:534–535. <http://dx.doi.org/10.1126/science.1165668>
- Hartzell, C., I. Putzier, and J. Arreola. 2005. Calcium-activated chloride channels. *Annu. Rev. Physiol.* 67:719–758. <http://dx.doi.org/10.1146/annurev.physiol.67.032003.154341>
- Hengl, T., H. Kaneko, K. Dauner, K. Vocke, S. Frings, and F. Möhrlein. 2010. Molecular components of signal amplification in olfactory sensory cilia. *Proc. Natl. Acad. Sci. USA*. 107:6052–6057. <http://dx.doi.org/10.1073/pnas.0909032107>
- Huang, F., X. Wong, and L.Y. Jan. 2012a. International Union of Basic and Clinical Pharmacology. LXXXV: Calcium-activated chloride channels. *Pharmacol. Rev.* 64:1–15. <http://dx.doi.org/10.1124/pr.111.005009>
- Huang, F., H. Zhang, M. Wu, H. Yang, M. Kudo, C.J. Peters, P.G. Woodruff, O.D. Solberg, M.L. Donne, X. Huang, et al. 2012b. Calcium-activated chloride channel TMEM16A modulates mucin secretion and airway smooth muscle contraction. *Proc. Natl. Acad. Sci. USA*. 109:16354–16359. <http://dx.doi.org/10.1073/pnas.1214596109>
- Huang, W.C., S. Xiao, F. Huang, B.D. Harfe, Y.N. Jan, and L.Y. Jan. 2012. Calcium-activated chloride channels (CaCCs) regulate action potential and synaptic response in hippocampal neurons. *Neuron*. 74:179–192. <http://dx.doi.org/10.1016/j.neuron.2012.01.033>
- Hwang, S.J., P.J. Blair, F.C. Britton, K.E. O'Driscoll, G. Hennig, Y.R. Bayguinov, J.R. Rock, B.D. Harfe, K.M. Sanders, and S.M. Ward. 2009. Expression of anoctamin 1/TMEM16A by interstitial cells of Cajal is fundamental for slow wave activity in gastrointestinal muscles. *J. Physiol.* 587:4887–4904. <http://dx.doi.org/10.1113/jphysiol.2009.176198>
- Jung, J., J.H. Nam, H.W. Park, U. Oh, J.H. Yoon, and M.G. Lee. 2013. Dynamic modulation of ANO1/TMEM16A HCO_3^- permeability by Ca^{2+} /calmodulin. *Proc. Natl. Acad. Sci. USA*. 110:360–365. <http://dx.doi.org/10.1073/pnas.1211594110>
- Kopelman, H., M. Corey, K. Gaskin, P. Durie, Z. Weizman, and G. Forstner. 1988. Impaired chloride secretion, as well as bicarbonate secretion, underlies the fluid secretory defect in the cystic fibrosis pancreas. *Gastroenterology*. 95:349–355.
- Kunzelmann, K., Y. Tian, J.R. Martins, D. Faria, P. Kongsuphol, J. Ousingsawat, L. Wolf, and R. Schreiber. 2012. Airway epithelial cells—functional links between CFTR and anoctamin dependent Cl^- secretion. *Int. J. Biochem. Cell Biol.* 44:1897–1900. <http://dx.doi.org/10.1016/j.biocel.2012.06.011>
- Liu, M., T.Y. Chen, B. Ahamed, J. Li, and K.W. Yau. 1994. Calcium-calmodulin modulation of the olfactory cyclic nucleotide-gated cation channel. *Science*. 266:1348–1354. <http://dx.doi.org/10.1126/science.266.5189.1348>
- Malvezzi, M., M. Chalal, R. Janjusevic, A. Picollo, H. Terashima, A.K. Menon, and A. Accardi. 2013. Ca^{2+} -dependent phospholipid scrambling by a reconstituted TMEM16 ion channel. *Nat Commun.* 4:2367. <http://dx.doi.org/10.1038/ncomms3367>
- Ni, Y.L., A.S. Kuan, and T.Y. Chen. 2014. Activation and inhibition of TMEM16A calcium-activated chloride channels. *PLoS ONE*. 9:e86734. <http://dx.doi.org/10.1371/journal.pone.0086734>
- Park, H.W., and M.G. Lee. 2012. Transepithelial bicarbonate secretion: Lessons from the pancreas. *Cold Spring Harb. Perspect. Med.* 2:a009571. <http://dx.doi.org/10.1101/cshperspect.a009571>
- Qu, Z., and H.C. Hartzell. 2000. Anion permeation in Ca^{2+} -activated Cl^- channels. *J. Gen. Physiol.* 116:825–844. <http://dx.doi.org/10.1085/jgp.116.6.825>
- Qu, Z., and H.C. Hartzell. 2001. Functional geometry of the permeation pathway of Ca^{2+} -activated Cl^- channels inferred from analysis of voltage-dependent block. *J. Biol. Chem.* 276:18423–18429. <http://dx.doi.org/10.1074/jbc.M101264200>
- Quinton, P.M. 2007. Cystic fibrosis: Lessons from the sweat gland. *Physiology (Bethesda)*. 22:212–225. <http://dx.doi.org/10.1152/physiol.00041.2006>
- Richman, D.P., Y. Yu, T.T. Lee, P.Y. Tseng, W.P. Yu, R.A. Maselli, C.Y. Tang, and T.Y. Chen. 2012. Dominantly inherited myotonia congenita resulting from a mutation that increases open probability of the muscle chloride channel CLC-1. *Neuromolecular Med.* 14:328–337. <http://dx.doi.org/10.1007/s12017-012-8190-1>
- Sakmann, B., and E. Neher. 1984. Patch clamp techniques for studying ionic channels in excitable membranes. *Annu. Rev. Physiol.* 46:455–472. <http://dx.doi.org/10.1146/annurev.ph.46.030184.002323>
- Scheele, G.A., S.I. Fukuoka, H.F. Kern, and S.D. Freedman. 1996. Pancreatic dysfunction in cystic fibrosis occurs as a result of impairments in luminal pH, apical trafficking of zymogen granule membranes, and solubilization of secretory enzymes. *Pancreas*. 12:1–9. <http://dx.doi.org/10.1097/00006676-199601000-00001>
- Schroeder, B.C., T. Cheng, Y.N. Jan, and L.Y. Jan. 2008. Expression cloning of TMEM16A as a calcium-activated chloride channel subunit. *Cell*. 134:1019–1029. <http://dx.doi.org/10.1016/j.cell.2008.09.003>
- Scudieri, P., E. Sondo, L. Ferrera, and L.J. Galiotta. 2012. The anoctamin family: TMEM16A and TMEM16B as calcium-activated chloride channels. *Exp. Physiol.* 97:177–183. <http://dx.doi.org/10.1113/expphysiol.2011.058198>
- Sigworth, F.J. 1983. Electronic design of the patch clamp. In *Single-Channel Recording*. B. Sakmann and E. Neher, editors. Plenum Press, New York. 3–35.
- Sohma, Y., M.A. Gray, Y. Imai, and B.E. Argent. 2001. 150 mM HCO_3^- —How does the pancreas do it? Clues from computer modelling of the duct cell. *JOP*. 2:198–202.

- Stephan, A.B., E.Y. Shum, S. Hirsh, K.D. Cygnar, J. Reisert, and H. Zhao. 2009. ANO2 is the cilia calcium-activated chloride channel that may mediate olfactory amplification. *Proc. Natl. Acad. Sci. USA*. 106:11776–11781. <http://dx.doi.org/10.1073/pnas.0903304106>
- Stöhr, H., J.B. Heisig, P.M. Benz, S. Schöberl, V.M. Milenkovic, O. Strauss, W.M. Aartsen, J. Wijnholds, B.H. Weber, and H.L. Schulz. 2009. TMEM16B, a novel protein with calcium-dependent chloride channel activity, associates with a presynaptic protein complex in photoreceptor terminals. *J. Neurosci.* 29:6809–6818. <http://dx.doi.org/10.1523/JNEUROSCI.5546-08.2009>
- Suzuki, J., M. Umeda, P.J. Sims, and S. Nagata. 2010. Calcium-dependent phospholipid scrambling by TMEM16F. *Nature*. 468:834–838. <http://dx.doi.org/10.1038/nature09583>
- Suzuki, J., T. Fujii, T. Imao, K. Ishihara, H. Kuba, and S. Nagata. 2013. Calcium-dependent phospholipid scramblase activity of TMEM16 protein family members. *J. Biol. Chem.* 288:13305–13316. <http://dx.doi.org/10.1074/jbc.M113.457937>
- Tarran, R., M.E. Loewen, A.M. Paradiso, J.C. Olsen, M.A. Gray, B.E. Argent, R.C. Boucher, and S.E. Gabriel. 2002. Regulation of murine airway surface liquid volume by CFTR and Ca²⁺-activated Cl⁻ conductances. *J. Gen. Physiol.* 120:407–418. <http://dx.doi.org/10.1085/jgp.20028599>
- Terashima, H., A. Picollo, and A. Accardi. 2013. Purified TMEM16A is sufficient to form Ca²⁺-activated Cl⁻ channels. *Proc. Natl. Acad. Sci. USA*. 110:19354–19359. <http://dx.doi.org/10.1073/pnas.1312014110>
- Tian, Y., P. Kongsuphol, M. Hug, J. Ousingasawat, R. Witzgall, R. Schreiber, and K. Kunzelmann. 2011. Calmodulin-dependent activation of the epithelial calcium-dependent chloride channel TMEM16A. *FASEB J.* 25:1058–1068. <http://dx.doi.org/10.1096/fj.10-166884>
- Vocke, K., K. Dauner, A. Hahn, A. Ulbrich, J. Broecker, S. Keller, S. Frings, and F. Möhrlein. 2013. Calmodulin-dependent activation and inactivation of anoctamin calcium-gated chloride channels. *J. Gen. Physiol.* 142:381–404. <http://dx.doi.org/10.1085/jgp.201311015>
- Xiao, Q., K. Yu, P. Perez-Cornejo, Y. Cui, J. Arreola, and H.C. Hartzell. 2011. Voltage- and calcium-dependent gating of TMEM16A/Ano1 chloride channels are physically coupled by the first intracellular loop. *Proc. Natl. Acad. Sci. USA*. 108:8891–8896. <http://dx.doi.org/10.1073/pnas.1102147108>
- Yang, H., A. Kim, T. David, D. Palmer, T. Jin, J. Tien, F. Huang, T. Cheng, S.R. Coughlin, Y.N. Jan, and L.Y. Jan. 2012. TMEM16F forms a Ca²⁺-activated cation channel required for lipid scrambling in platelets during blood coagulation. *Cell*. 151:111–122. <http://dx.doi.org/10.1016/j.cell.2012.07.036>
- Yang, Y.D., H. Cho, J.Y. Koo, M.H. Tak, Y. Cho, W.S. Shim, S.P. Park, J. Lee, B. Lee, B.M. Kim, et al. 2008. TMEM16A confers receptor-activated calcium-dependent chloride conductance. *Nature*. 455:1210–1215. <http://dx.doi.org/10.1038/nature07313>
- Yu, K., J. Zhu, Z. Qu, Y.Y. Cui, and H.C. Hartzell. 2014. Activation of the Ano1 (TMEM16A) chloride channel by calcium is not mediated by calmodulin. *J. Gen. Physiol.* 143:253–267. <http://dx.doi.org/10.1085/jgp.201311047>
- Zhang, X.D., P.Y. Tseng, W.P. Yu, and T.Y. Chen. 2009. Blocking pore-open mutants of CLC-0 by amphiphilic blockers. *J. Gen. Physiol.* 133:43–58. <http://dx.doi.org/10.1085/jgp.200810004>